Structural and dielectric characterization of Potassium diphosphate/Hydroxyapatite ceramic biocomposite

M. I. Pérez-Valverde[a,*], O. García-Zaldívar[b], and M. E. Mendoza[a]

[a] *Instituto de Física "Luis Rivera Terrazas", Benemérita Universidad Autónoma de Puebla, Av. San Claudio y 18 sur, Edif. IF-2, Ciudad Universitaria. Puebla, Pue., 72570, México.*

[*] *Coordinación para la Innovación y Aplicación de la Ciencia y Tecnología, Universidad Autónoma de San Luis Potosí, Álvaro Obregón 64, San Luis Potosí 78000, México.*

e-mail: maritza.iveth.perez@gmail.com; emendoza@ifuap.buap.mx

[b] *Grupo de Materiales Ferroicos de Facultad de Física/Instituto de Ciencia y Tecnología de Materiales, Universidad de La Habana, San Lázaro y L, Vedado, Plaza, La Habana 10400, Cuba.*

e-mail: osmany.garcia@gmail.com

Received 24 May 2023; accepted 5 September 2023

We study the KH_2PO_4(KDP)/$Ca_{10}(PO_4)_6(OH)_2$ (HA) biocomposite to evaluate its electrical conductivity. It was prepared by manual grinding on a 1:3 molar ratio. Studies by X-ray powder diffraction and Raman spectroscopy show a variation in the volume of the unit cell between KDP and HA and the disappearance of bands associated with KDP. Impedance spectroscopy was studied over a range of temperatures (25-80°C) and frequencies from 10 Hz to 1 MHz. It was found that the bulk resistance of the composite is higher in pure KDP. Using the Jonscher empirical expression suggest that the ionic hopping conduction mechanism is responsible for the conductivity behavior with hopping frequency of $1.21 \times 10_4$ Rad at 80°C.

Keywords: Composites; apatite; proton hopping; impedance.

DOI: https://doi.org/10.31349/RevMexFis.70.021001

1. Introduction

Hydrogen bonding materials are an interesting research topic because of its fundamental importance in many branches of science, for example, in medicine as prosthetics, in optics as generation of second harmonic, in electronics as piezoelectric material to name a few [1]. Furthermore, hydrogen bonding is central to understand microscopic structures and functions in many molecular and supramolecular systems [2]. Potassium dihydrogen phosphate (KH_2PO_4 abbreviated hereinafter as KDP) is an inorganic ferroelectric compound containing hydrogen bonds responsible for its ferroelectric properties. It has a Curie temperature of $T_c = -150.15$°C [3] and above this temperature it changes to a paraelectric state. In the ferroelectric phase it can be described by the space group Fdd2, unit cell parameters $a = 10.544(7)$Å $b = 10.481(6)$Å $c = 6.920(5)$Å $volume = 764.74(6)$Å^3 [4], with spontaneous polarization of $P_s = 5.1$ μ/cm^2 in the c axis of its unit cell [5]. In its paraelectric phase it can be described by the I-42d space group symmetry, with the lattice parameters of $a = b = 7.4521(4)$Å $c = 6.974(2)$Å $volume = 387.29$Å^3 [6]. In this paraelectric phase, the hydrogen atoms are randomly distributed between two equivalent minima of the double-well potential [7]. Conductivity on the KDP is determined by the proton transport within the framework of hydrogen bonds thought three types of defects: ionization, L and D defects [8] represented in Fig. 1. The ionization defect is due to the production of $(HPO_4)^{2-}$ and (H_3PO_4) as the proton jumps from one PO_4 group to another along the same bond, illustrated in Fig. 1a). The L and D defects are produced when a proton jumps between different H-O bonds on the same PO_4 group, this can leave a hydrogen bond without a proton (L defect) and produce a bond with a proton in each of its two proton positions (D defect) [9], as illustrated in Fig. 1b).

In our previous work, we demonstrate that the mechanism of conductivity in KDP in a composite with p-benzoquinone remains, however, we found that the activation energy of proton hopping reduces on increasing p-benzoquinone concen-

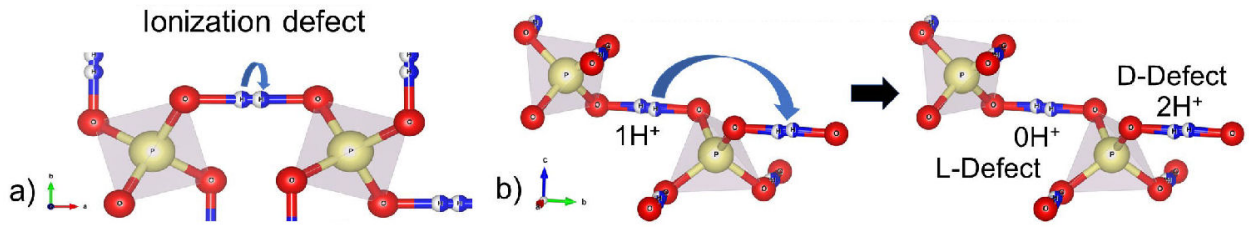

FIGURE 1. Schematic representation of conductivity on paraelectric KDP. This figure was generated using VESTA software [10].

tration [11]. Hydroxyapatite, ($Ca_{10}(PO_4)_6(OH)_2$ hereafter abbreviated as HA) is the principal inorganic constituent of teeth and is chemically and structurally similar to the mineral portion of bones [12]. The crystal structure of HA most frequently encountered is hexagonal, described by the $P6_3/m$ space group, with lattice parameters $a = b = 9.4239(1)$ Å, $c = 6.8841(1)$Å, $volume = 529.47$ Å^3 [13]. It has a lattice of hydroxyl ions (OH^-) aligned in columns parallel to the c-axis, along with Ca^{2+} and (PO_4^{3-}) ions [14]. HA can also exist in the monoclinic structure, described by the space group $P2_1/b$, it has lattice parameters $a = 9.426(3)$ Å, $b = 6.887(1)$ Å, $c = 18.856(5)$, $c = 6.887(1)$ Å, $\gamma = 119.97(1)$ ° $volume = 1060.40$ Å^3 [15]. The major difference between the monoclinic HA and the hexagonal HA is the orientation of the hydroxyl groups. In the monoclinic HA, all of the OHs in a given column are pointed in the same direction, and the direction reverses in the next column. On the other hand, in the hexagonal HA, the adjacent OHs point in the opposite directions of the monoclinic structure [16].

The ionic conductivity in HA is mediated via various pathways, including (i) jumping of OH^- ions (ii) conduction through O^{2-} and (iii) conduction through H^+. The activation energy (E_a) for the jump of OH^- ions along the c-axis was ($2 - 2.1$ eV), for O^{2-} 1.5 eV, and for H^+ ion conduction 0.5 eV [14,17,18]. Nagai and Nishino [19] indicated that at room temperature conduction is due to migration of H^+ in adsorbed water. Conductivity at elevated temperatures is described through jumping of OH^-, since the OH^- vacancies formed during dehydration are likely to obstruct H^+ conduction and facilitate OH^- conduction [14,17].

The aim of the present work is the study of the conductivity of KDP in a composite with $Ca_{10}(PO_4)_6(OH)_2$ (HA). It can be expected a modification of conductivity in the composite, due to the fact that both of these phosphates have a proton conduction mechanism. We explore its structure with X-ray diffraction and Raman spectroscopy and the electric properties using impedance spectroscopy. Moreover, we study the behavior of permittivity, dielectric loss and conductivity with temperature to identify the stability of the composite.

2. Materials and methods

Composite was prepared with molar ratio of 1:3 (KDP:HA, labeled 1K3HA, here and after) by manual grinding in a glove box in nitrogen atmosphere, using potassium dihydrogen phosphate, KH_2PO_4 (KDP) (99.3%, J.T. Baker ACS) . HA powders were synthesized using the sol-gel method assisted by ultrasonic irradiation as described in [20]. Corresponding quantities of KDP and HA were used for the preparation.

Phase identification of the composite and pure components were characterized by X-ray powder diffraction using a PANalytical Empyrean diffractometer operating at 45 kV/40 mA and Cu Kα radiation with a Nickel filter to ensure that only Kα radiation was interacting with the samples. The diffraction patterns were obtained in the 10-90° (2θ) angular range, 0.004° step size and 63.230 s scan step time. A rotating sample-holder prevented preferred orientation effects. Rietveld refinement was performed to determine the lattice parameters using X'Pert HighScore Plus 2.2.2. The refined parameters were zero shift, background, scale factor, lattice parameters, atomic thermal factors and UVW. Raman spectra were obtained with a Horiba JobinYvon HR800 microspectrometer, an OLYMPUS BX41 microscope and a thermoelectrically cooled CCD detector; the 632.8 nm emission of a He–Ne laser was employed as the excitation source; all data were collected at room temperature.

The impedance study was performed in a Precision Impedance Analyzer Agilent 4294A from 500 Hz to 1 MHz. Powders were pressed into pellets, then, silver paste were deposited and cured on both sides of the pellets to be used as electric contacts. Measurements were made from room temperature to a maximum temperature of 80°C the data were collected during the cooling cycle. From the obtained impedance data, permittivity ε', dielectric losses ($\tan\delta$) and AC conductivity (σ_{ac}) were obtained by means of the following equations: $\varepsilon^{'} = (t/\omega A\varepsilon_0)(-Z''/Z'^2 + Z''^2)$ where, ω is the angular frequency ($\omega = 2\pi f$), ε_0 is the permittivity of free space 8.854×10^{-12} F/m, t is the thickness of the sample and A is the area of the electric contacts, $\tan\delta = -Z'/Z''$ and $\sigma_{ac} = (t/A)(Z'/[Z'^2 + Z''^2])$ [14].

3. Results and discussion

3.1. X-ray diffraction

The X-ray powder diffraction patterns of KDP, HA and 1K3HA composite were normalized and are shown in Fig. 2. Peaks marks with (*) and (°) correspond to KDP and HA phases respectively. With the used methodology for the synthesis of HA it was expected to have mixed hexagonal-monoclinic phases of HA [21]. We consider monoclinic and hexagonal phases in the HA used in this work as well. The sharp diffraction peaks observed in pattern is indicative of the high crystallinity of the obtained samples. All diffraction peaks were indexed considering the powder diffraction files 01-084-0520, 01-089-4405 and 04-007-5086 for KDP, monoclinic HA and hexagonal HA respectively, no discernable peaks of additional phases apart of tetragonal KDP, monoclinic and hexagonal HA were found in the composite. In addition, it was observed that the relative intensity of peaks indexed to KDP in the composite were lower than in the pure phase of KDP, this corresponds to the molar ratio with which the composite was prepared.

Rietveld refinements were performed in the pure components and in the composite using standard PDF file references for KDP (01-084-0520), monoclinic HA (01-089-4405) and hexagonal HA (04-007-5086). To measure the agreement between the crystallographic model and the experimental X-ray diffraction data it is useful to have agreement indices as the

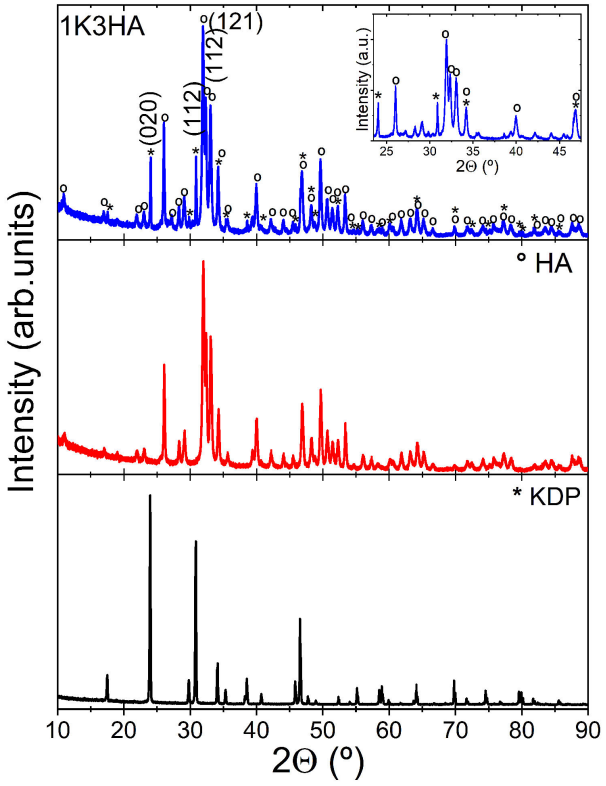

FIGURE 2. X-ray diffraction patterns for KDP, HA and 1K3HA.

weighted profile R-factor (R_{wp}). The weighted profile R-factor (R_{wp}) obtained with the refinement were $R_{wp} = 9.09$, 8.84, and 8.08 for KDP, HA, and for the 1K3HA composite respectively. The values of the agreement indexes are less than 10 resulting in acceptable refinements. Rietveld refinement of lattice parameters of the phases found in the XRD pattern of 1K3HA composite are presented in Table I. The percentage of volume change ($\Delta V/V_i$(%)) respected to the pure experimental KDP and HA is lower on HA than in KDP indicating that the KDP could experiment a slight expansion due to the interaction with HA. Moreover, the quantification of phases with Rietveld refinement (W_i(%)) gives the relation $\sim 1:3$ of KDP:HA, with the majority of the HA in the monoclinic phase, corroborating the proposed molar relationship. To identify small changes in the local structure of the composite Raman spectroscopy was done.

3.2. Raman spectroscopy

The Raman spectra of pure components and composite were normalized to allow a better comparison, they are shown in Fig. 3. The Raman spectra of HA mainly consist of four scattering bands, which are associated with four frequencies (υ_1, υ_2, υ_3, and υ_4) of the PO_4 group [22,23]. Bands at 435 cm^{-1} and 454 cm^{-1} are attributed to the doubly degenerate bending mode (υ_2) of the PO_4 group (O-P-O bond). Peaks ranging from 580 to 620 cm^{-1} correspond to bending mode (υ_4) of the PO_4 group (O-P-O bond). A very strong peak in

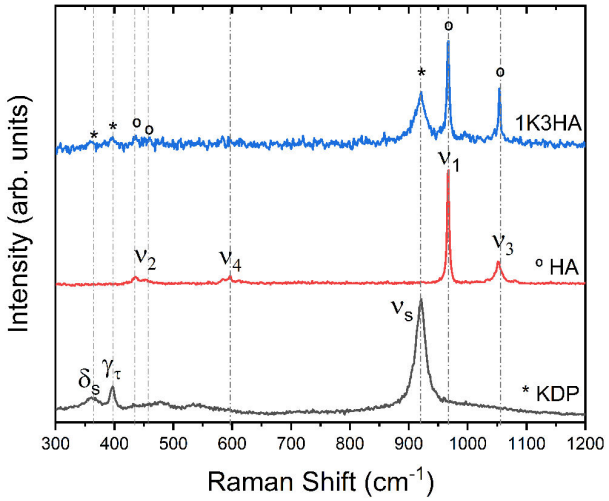

FIGURE 3. Raman spectra comparison of composite with pure KDP, HA and 1K3HA composite.

TABLE I. Rietveld refinement of 1K3HA composite.

1K3HA	a (Å)	b (Å)	c (Å)	γ(°)	Volume (Å^3)	$\Delta V/V_i$(%)	W_i(%)
KDP	7.4560(1)	7.4560(1)	6.9754(2)		387.79	0.12	8.8
HA hexagonal	9.4272(2)	9.4272(2)	6.8838(2)	120	529.82	0.06	23.1
HA monoclinic	9.4526(5)	6.8853(3)	18.8154(1)	119.986(6)	1060.68	0.02	68.2
PDF files used for refinement							
KDP PDF 01-084-0520	7.4521(4)	7.4521(4)	6.974(2)		387.29		
HA hexagonal PD F04-007-5086	9.4239(1)	9.4239(1)	6.8841(1)	120	529.47		
HA monoclinic PDF 01-089-4405	9.426(3)	6.887(1)	18.856(5)	119.97(1)°	1060.40		

967 cm^{-1} is assigned to the symmetric stretching mode (υ_1) of the PO_4^{-3} tetrahedron. The bands in the range between 1050 and 1085 cm^{-1} are assigned to the triply degenerate asymmetric stretching mode (υ_3) of the PO_4 group (P-O bond). The Raman spectra of KDP consist of a principal and relativity narrow mode located at 921.5 cm^{-1}, related to symmetrical stretching (*vs*) of $P(OH)_2$ and four others less intense modes at lower frequencies [24]. The band observed at 362 cm^{-1} correspond to a symmetrical in plane bending (δ_s) of PO_2, $P(OH)_2$. At 397 cm^{-1} twisting out of plane bending (γ_τ) of $P(OH)_2$. The band located at 478 cm^{-1} corresponds to an asymmetrical in plane bending (δ) of PO_2, $P(OH)_2$. At 541 cm^{-1} wagging out of plane bending (γ_ω) $P(OH)_2$.

In the composite, no modes related to the appearance of new chemical bonds are observed, instead, some of the characteristic modes present in KDP and HA can be observed. Six modes in total were observed, three very weak modes at low frequencies (360-440 cm^{-1}) and three strong modes at frequencies 850-1100 cm^{-1}. The assignation of modes for 1K3HA sample is the following, mode at 362.14 cm^{-1} corresponds to bending in plane of PO_2, $P(OH)_2$, mode at 396.94 cm^{-1} is an out of plane bending of $P(OH)_2$ assigned both to KDP, at 435.97 cm^{-1} bending of the O-P-O (υ_2) in PO_4^{-3} assigned to HA; follow by strong modes, symmetrical stretching of $P(OH)_2$ at 921.5 cm^{-1} of KDP, stretching of the P-O band in PO_4^{-3} at 967.61 cm^{-1} of HA and lastly a band at 1052.96 cm^{-1} of the asymmetric stretching mode (ν_3) of the PO_4 group (P-O bond) PO_4^{-3} which correspond to HA mode. It was noticeable that the relative intensity of the (ν_3) mode increased when compared to pure HA. In the composite its intensity is higher (25%) than in pure HA, this could be explained as a consequence of an increase of P – O bond length in the composite, as reported in [25] they found a correlation between the mean asymmetric wavenumber and the P – O bond in PO_4 group in some aminoacids.

As occurs in the obtained diffraction patterns, the relative intensities of the modes assigned to KDP in the compound decrease compared to the pure component, this is due to the majority of molar proportion of HA. The bending mode (υ_4) of the PO_4 group (O-P-O bond) of HA as well as the in plane bending (δ) mode of PO_2, $P(OH)_2$ and wagging out of plane bending (γ_ω) $P(OH)_2$ mode of KDP were not distinguishable in the spectrum.

As can be observed, there is no shift in frequency modes measured in the composite compared to that measured in pure KDP and HA materials, indicative that there is no modification in the existing chemical bonds. Hence, no chemical interaction between KDP and HA are appreciable in the composite.

3.3. Impedance spectroscopy

The electrical properties, especially the conductive processes, which is governed by the hydrogen bonds, is of particular interest. Firstly, we analyzed the behavior on impedance, dielectric modulus, permittivity and dielectric loss, afterwards the dc and ac conductivity and its mechanism of conductivity.

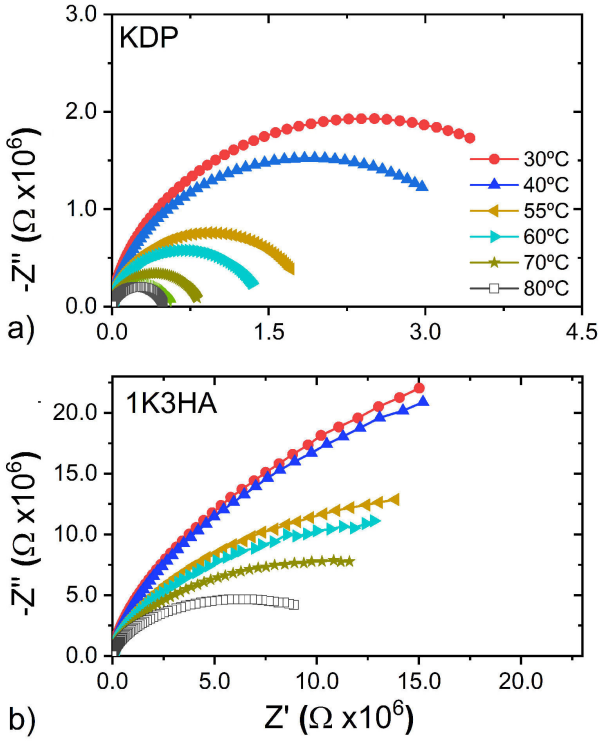

FIGURE 4. Nyquist plot of a) KDP and b) 1K3HA composite.

The Nyquist plots of KDP and 1K3HA composite as a function of temperature are shown in Fig. 4. Single arcs, typical of systems with a single conduction mechanism, can be observed. The limited frequency range was the major reason behind the incomplete semicircle (at low frequencies) obtained in the Nyquist plot for lower temperatures. The radius of the semicircles, for both the KDP and 1K3HA, decreases with temperature due to an increase in the conductivity of the samples. The bulk resistance (semicircle diameter on the Nyquist plot [26,27]) of the 1K3HA composite is higher than that observed in pure KDP in the entire temperature range studied, meaning the resistivity in the composite gets a higher value.

The simultaneous study of complex impedance (Z*) and complex modulus (M*) provides the entire spectrum of conduction mechanism, *i.e.*, long range (from Z*) as well as localized conduction (from M*) occurring in the dielectric materials [28]. The values of real and imaginary components of electric modulus (M) have been calculated using the relationship, $M' = 2\pi f C_0 Z''$, $M'' = 2\pi f C_0 Z'$; where, f and C_0 are the frequency and geometric capacitance ($C_0 = \varepsilon_0 A/t$), respectively [27]. Impedance and modulus spectroscopic plots at different temperatures for KDP and 1K3HA are shown in Fig. 5. Well-defined peaks are observed. The maximum values of impedance and modulus take place at different frequencies, representing the involvement of a number of relaxation processes (distribution of relaxations times) or non-Debye type behavior in the samples due to materials in-

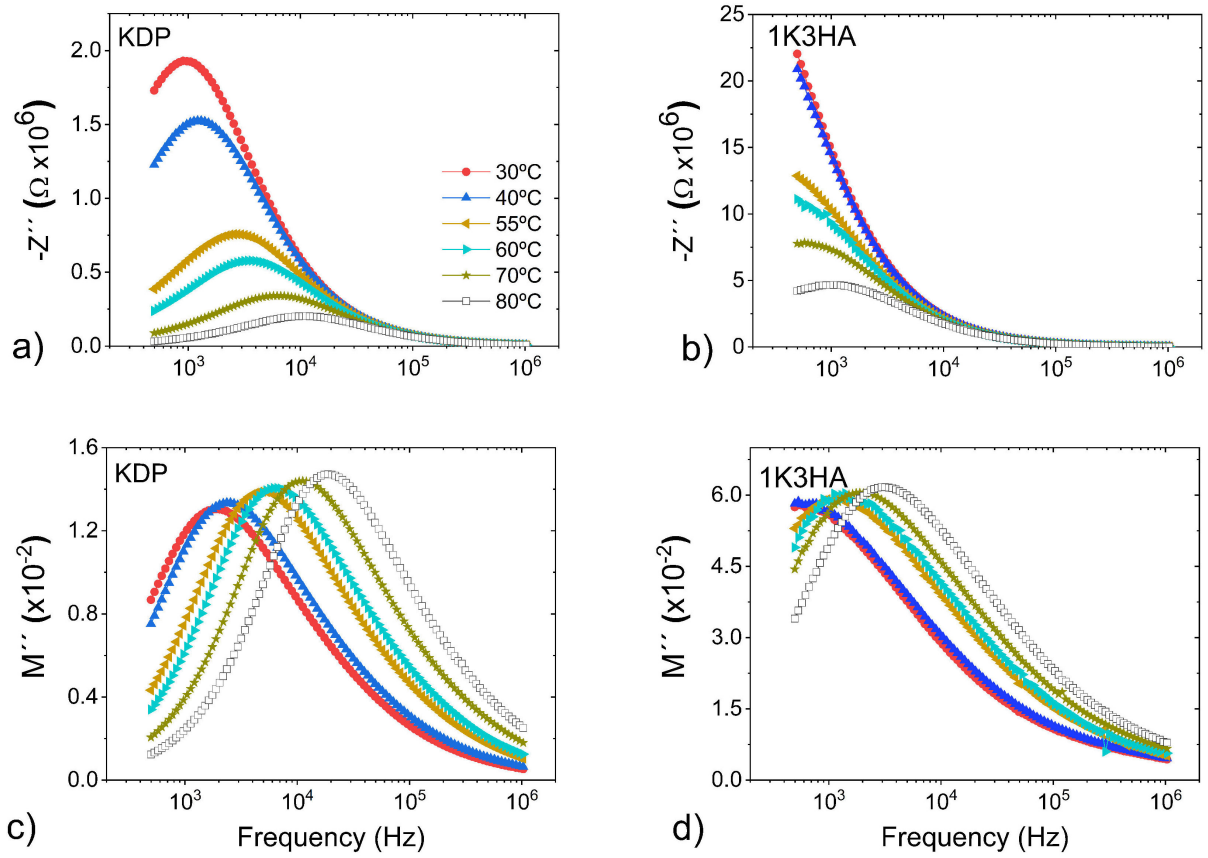

FIGURE 5. Impedance and modulus spectroscopic plots for KDP (a and c), and 1K3HA composite (b and d) at various temperatures.

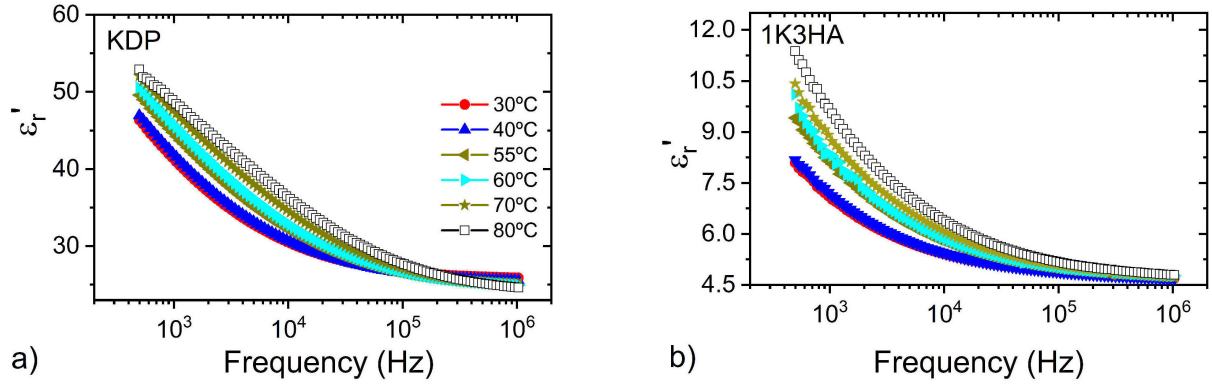

FIGURE 6. Frequency dependence of dielectric constant spectra at several temperatures of a) KDP and b) 1K3HA.

homogeneities [28]. In the spectroscopic plots, the shift of the peak towards lower frequencies as the temperature decrease, as can be observed in Fig. 5, implies an increase in relaxation times [27]. The variations in peak position and height with temperature suggest that the dominant conduction mechanism is probably the hopping of charge carriers due to thermal activation [29].

Figures 6a), b) show the variation in the real part of relative permittivity as a function of frequency at a few isothermal temperatures from room temperature to 80°C. The dielectric constant decreases with increase in frequency and this dielectric dispersion with frequency is more significant at higher temperatures and lower frequencies representing the relaxation of interfacial or space charge polarization. At low frequency (5 kHz) and at low temperature all the mechanisms of polarization contribute, but as the frequency increases the contribution from different polarization mechanisms starts to decrease. At low frequency (5 kHz) and at higher temperature, the dielectric constant has a much larger value, thereby indicating the contribution of space charge polarization which decreases as the frequency. Thus, this type of behavior indicates higher space charge polarizability of

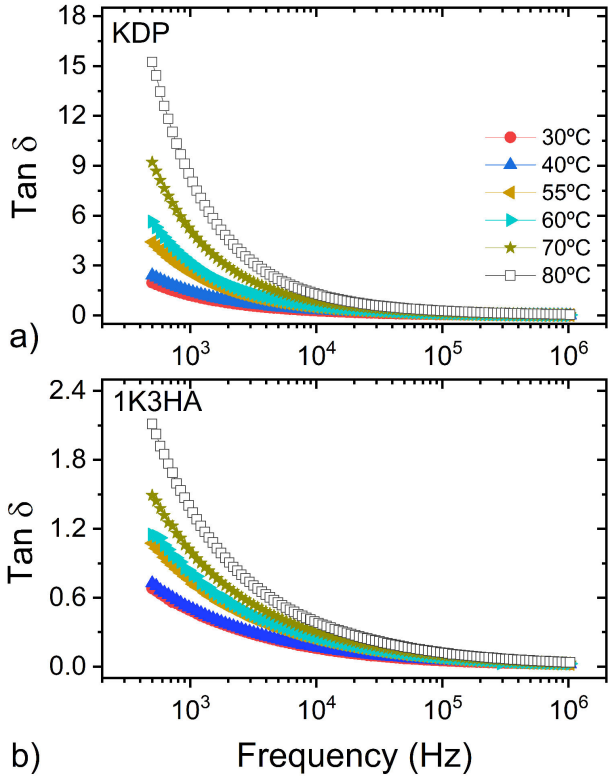

FIGURE 7. Frequency dependence of dielectric loses spectra at a few temperatures for a) KDP and b)13HA composite.

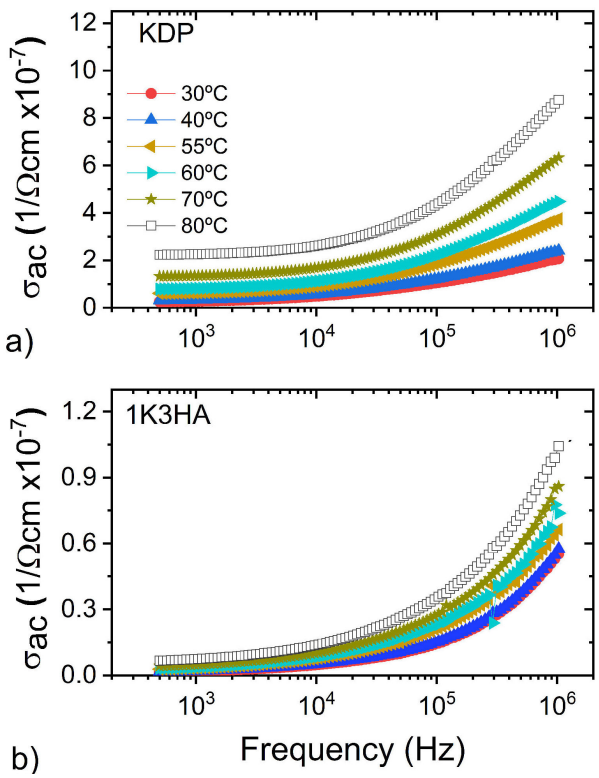

FIGURE 8. Variation of ac conductivity with frequency for a) KDP and b) 1K3HA composite.

the material in the lower frequency and at higher temperature range. The dielectric dispersion decrease at higher frequencies (above 10^5 Hz) because of the applied electric field is much higher than the natural frequency of some polarization mechanism and, therefore such the dipoles do not have the chance to react and consequently does not contribute to the dielectric constant. Also, the dispersion in the dielectric constant in the low frequency (< 1 kHz) and high temperature range is indicative of the presence of dc conductivity in the samples [30,31].

The dielectric loss ($\tan\delta$) gradually decreases with frequency as shown in Fig. 7, indicating that the conductive component has a greater contribution than the dipolar component. This is because the fundamental mechanism of conduction is associated with the hopping of ions and there is no strong contribution due to intrinsic dipoles.

The nature of ac conductivity (σ_{ac}) is shown in Fig. 8. The frequency dependence of conductivity is a sum of dc conductivity due to movements of free charges and polarization conductivity due to local displacement of bounded charges [32]. The room temperature ac conductivity values for KDP and 1K3HA sample at a frequency of 10 kHz are 4.7×10^{-8} and 5.89×10^{-9} $(\Omega\text{cm})^{-1}$ respectively. The low temperature process is associated with motions of OH^- ions in the HA phase of the ceramic [33,34]. The low-conductivity value at low frequencies is related to the accumulation of ions due to the slow periodic reversal of the electric field [32]. It has been demonstrated that the proton migration in water, adsorbed on the surface of HA, is one of the important factors responsible for the conduction in the lower temperature region ($< 100°$C) [14,19]. It has been reported that the adsorbed water layer can lead to conduction paths, which take place by means of a Grotthuss chain reaction in which protons are transferred from one water molecule to the next on the ceramic surface of HA [35]. Conductivity on the KDP is determined by the proton transport within the framework of hydrogen bonds [8], therefore, it is presumed that in the composite the conductivity in that temperature range is still due to proton conduction.

The variation of ac conductivity with frequency show a typical ionic conductivity behavior due to the hopping and vibrational mode of the ions. There is an increase in conductivity with the frequency following the $\sigma_{ac}(\omega) \propto (\omega)^s$ power law and such behavior is attributed to the relaxation of the mobile ion hopping. The frequency dependent ac conductivity, $\sigma(\omega)$ at a given frequency ω, is well described by the Jonscher empirical expression [36]: $\sigma_{ac} = \sigma_{dc} + B\omega^s$ $(0 \leq s < 1)$, $B = (\sigma_{dc}/\omega_H{}^s)$ where σ_{dc} is the direct current conductivity and s is a fractional angular frequency exponent characterizing the power law behavior [37], the value of s is in the range of 0 and 1, ω_H is the hopping frequency of charge carriers. This law corresponds to the short range hopping of charge carriers through trap sites that are separated by energy barriers of varied heights [38]. At low frequencies ($\omega < \omega_H$), the electrical conductivity $\sigma_{ac}(\omega)$, originates from the migration of ions, and at at high frequencies ($\omega < \omega_H$) due to the same ionic transport mechanism [37].

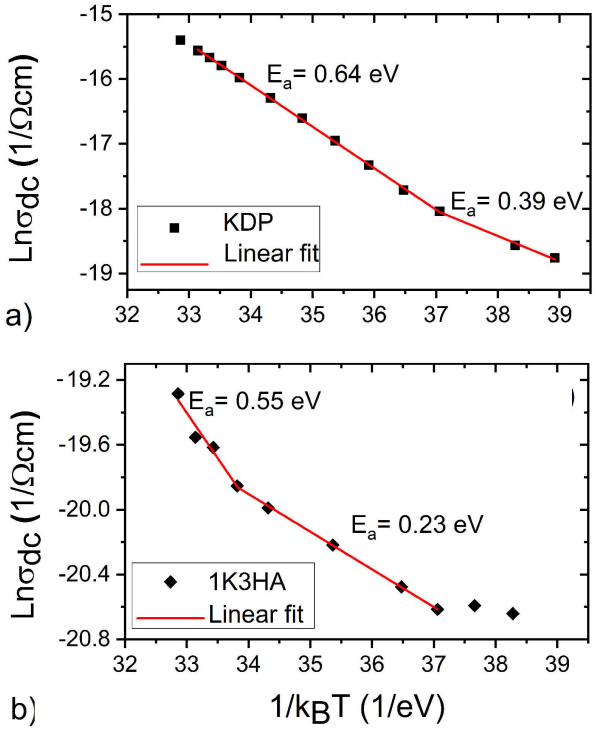

FIGURE 9. Variation of dc conductivity with temperature for a) KDP and b) 1K3HA composite.

The frequency dependent conductivity spectra of KDP and 1K3HA were fitted to Jonscher empirical expression. In the fitting process, σ_{dc}, ω_H and s were varied simultaneously to get the best fits. The fitting function and the experimentally recorded data were in reasonable agreement over a large frequency range (500 Hz–300 kHz). We found that the value of s varies from 0.335 to 0.56 for KDP and from 0.57 to 0.50 for the 1K3HA composite in the temperature range measured, hence, suggesting that the ionic hopping conduction mechanism is responsible for the conductivity behavior [39,40]. It has been found that most of the compounds exhibiting proton conduction have strong hydrogen bonds so that the protons can move through the hydrogen bond channels [41].

The dc conductivity of samples has been illustrated in Fig. 9. It is clear that the influence of KDP in the composite on dc conductivity is dependent on temperature, while the same order of magnitude is recorded in the KDP and in the composite, but σ_{dc} increases with temperature. The room temperature dc conductivity values, obtained from the power law expression, for KDP and 1K3HA are 7.13×10^{-9} and 1.08×10^{-9} $(\Omega\text{cm})^{-1}$, respectively. The dc conductivity is found to be in the same order of magnitude in comparison with as observed frequency-dependent conductivity data. It suggests that ionic conduction predominates the dc conductivity.

The temperature dependence of the electrical dc conductivity was adjusted by the Arrhenius expression. Two conduction mechanisms with different activation energies (one at low temperature and one at higher temperature) were detected. The activation energy of KDP is comparable with the previous reported [42]. For the 1K3HA the activation energies have a lower value of activation energies compared to the pure KDP. At low temperature the activation energy in the 1K3HA sample could be associated with the migration of H^+ in adsorbed water as occurs in pure HA. In the high temperature range, the conduction mechanism could be due to the ionic conduction of H^+, since the value obtained for Ea, 0.55 eV, corresponds to that reported for pure HA, in addition, the value of Ea for the L defect mobility, conduction mechanism in the KDP, produced when a proton jumps between different H-O bonds on the same PO_4 group leaving an hydrogen bond without a proton is 0.53 eV [9] confirming the ionic conduction by H^+. The hopping frequency ω_H obtained by the Jonscher fitting was found to increase with temperature, figure not shown. The ω_H obtained for KDP was 5.42×10^5 Rad while for 1K3HA composite was 1.21×10^4 Rad at 80°C. The electrical conduction decreases due to the decreased hopping rate of charge carriers with increasing temperature.

4. Conclusions

In this work, we analyzed the effects of hydrogen bonds on the electrical properties of the composite 1K3HA. Potassium dihydrogen phosphate (KDP) and Hydroxyapatite (HA) were used. X-ray diffraction allows us to identify a mix of phases in the composite, the tetragonal KDP and monoclinic-hexagonal phases of HA. Raman spectroscopy indicates the interaction on the composite through missing bands of KDP and HA.

By studying impedance spectroscopy was found that the bulk resistance of the 1K3HA composite is higher than that observed in pure KDP in the entire temperature range studied. The variations in peak position and height with temperature on the impedance and modulus spectroscopic plots suggest that the dominant conduction mechanism is probably the hopping of charge carriers due to thermal activation. The dispersion in the dielectric constant in the low frequency (< 1 kHz) and high temperature range was indicative of the presence of dc conductivity. Using the Jonscher empirical expression, the value of 's' was < 1, thereby suggesting that the ionic hopping conduction mechanism is responsible for the conductivity behavior. Moreover, the dc conductivity obtained from the power law expression was found lower than in the KDP. The hopping frequency obtained by the Jonscher fitting of the composite is less than in KDP meaning that the electrical conduction decreases due to the decreased hopping rate of charge carriers with increasing temperature. In general, the composite is less conductive than the pure KDP and the mechanism of ionic conduction is the mobility of H^+.

Acknowledgments

The authors are thankful to the Mexican National Council of Science, and Technology (CONACYT) for financial support, to M.J. Robles-Águila CIDS-ICUAP and R. Pérez-Solís IQ-

UNAM for the preparation of HA and to L. Rojas IFUAP for manuscript revision.

1. K. L. Han and G. J. Zhao, Hydrogen Bonding and Transfer in the Excited State, 1st. ed. (John Wiley & Sons, Ltd, Chichester, UK, 2011), pp.1-452.
2. G. J. Zhao and K. L. Han, Hydrogen bonding in the electronic excited state, *Acc. Chem. Res*. **45** (2012) 404. https://doi.org/10.1021/ar200135h.
3. J. E. Diosa, R. A. Vargas, I. Albinsson, and B. E. Mellander, Dielectric relaxation of KH_2PO_4 above room temperature, *Phys. Status Solidi B* **241** (2004) 1369. https://doi.org/10.1002/pssb.200302000.
4. T. Miyoshi, H. Mashiyama, T. Asahi, H. Kimura, and Y. Noda, Single-crystal neutron structural analyses of potassium dihydrogen phosphate and potassium dideuterium phosphate, *J. Phys. Soc. Japan*. **80** (2011) 1. https://doi.org/10.1143/JPSJ.80.044709.
5. G. A. Samara, The effects of deuteration on the static ferroelectric properties of KH_2PO_4 (KDP), *Ferroelectrics* **5** (1973) 25. https://doi.org/10.1080/00150197308235776.
6. J. E. Tibballs and R. J. Nelmes, The crystal structure of tetragonal KH_2PO_4 and KD_2PO_4 as a function of temperature and pressure, *J. Phys. C: Solid State Phys.* **15** (1982)59.
7. J. C. Slater, Theory of the transition in KH2PO4, *J. Chem. Phys*. **99** (1941) 16. https://doi.org/10.1063/1.1750821.
8. M. O'Keeffe and C. T. Perrino, Proton conductivity in pure and doped KH2PO4, *J. Phys. Chem. Solids* **28** (1967) 211. https://doi.org/10.1016/0022-3697(67)90110-2.
9. L.B. Harris and G.J. Vella, Direct current conduction in ammonium and potassium dihydrogen phosphate, *J. Chem. Phys.* **58** (1973) 4550. https://doi.org/10.1063/1.1679018.
10. F. Momma and K. Izumi, VESTA 3 for three-dimensional visualization of crystal, volumetric and morphology data, *J. Appl. Crystallogr*. **44** (2011) 1272.
11. M. I. Pérez-Valverde, J. J. Gervacio-Arciniega, J. M. Siqueiros, and M. E. Mendoza, Dielectric and structural characterization and effective piezoelectric coefficient of KDP/p-Benzoquinone ceramic composites, *Ceram. Int.* **45** (2019) 9986. https://doi.org/10.1016/j.ceramint.2019.02.042.
12. B. Yilmaz, A. Z. Alshemary, and Z. Evis, Co-doped hydroxyapatites as potential materials for biomedical applications, *Microchem. J.* **144** (2019) 443. https://doi.org/10.1016/j.microc.2018.10.007.
13. L. Veselinović *et al*., IUCr, Crystal structure of cobalt-substituted calcium hydroxyapatite nanopowders prepared by hydrothermal processing, *J. Appl. Crystallogr.* **43** (2010) 320. https://doi.org/10.1107/S0021889809051395.
14. J. P. Gittings *et al*., Electrical characterization of hydroxyapatite-based bioceramics, *Acta Biomater.* **5** (2009) 743. https://doi.org/10.1016/j.actbio.2008.08.012.
15. T. Ikoma, A. Yamazaki, S. Nakamura, M. Akao, Preparation and Structure Refinement of Monoclinic Hydroxyapatite, *J. Solid State Chem.* **144** (1999) 272. https://doi.org/10.1006/jssc.1998.8120.
16. G. Ma and X. Y. Liu, Hydroxyapatite: Hexagonal or monoclinic?, *Cryst. Growth Des.* **9** (2009) 2991. https://doi.org/10.1021/cg900156w.
17. T. Yamashita, K. Kitagaki and K. Umegaki, Thermal Instability and proton conductivity of ceramic hydroxyapatite at high temperatures, *J. Am. Ceram. Soc.* **78** (1995) 1191.
18. M. S. Khalil, H. H. Beheri, W. I. Abdel Fattah, Structural and electrical properties of zirconia/hydroxyapatite porous composites, *Ceram. Int.* **28** (2002) 451. https://doi.org/10.1016/S0272-8842(01)00118-3.
19. M. Nagai and T. Nishino, Surface conduction of porous hydroxyapatite ceramics at elevated temperatures, *Solid State Ion.* **28-30** (1988) 1456. https://doi.org/10.1016/0167-2738(88)90403-1.
20. A. K. Sánchez-Hernández, J. Martínez-Juárez, J.J. Gervacio-Arciniega, R. Silva-González, and M.J. Robles-Águila, Effect of ultrasound irradiation on the synthesis of hydroxyapatite/titanium oxide nanocomposites, *Crystals* **10** (2020) 1. https://doi.org/10.3390/cryst10110959.
21. R. Pérez-Solis, J.J. Gervacio-Arciniega, B. Joseph, M.E. Mendoza, and A. Moreno, Synthesis and characterization of a monoclinic crystalline phase of hydroxyapatite by synchrotron X-ray powder diffraction and piezoresponse force microscopy, *Crystals* **8** (2018)458. https://doi.org/10.3390/cryst8120458.
22. A.F. Khan *et al*., Raman spectroscopy of natural bone and synthetic apatites, *Appl. Spectrosc. Rev.* **48** (2013) 329. https://doi.org/10.1080/05704928.2012.721107.
23. G. Penel, G. Leroy, C. Rey, and E. Bres, MicroRaman spectral study of the PO4 and CO3 vibrational modes in synthetic and biological apatites, *Calcif. Tissue Int.* **63** (1998) 475. https://doi.org/10.1007/s002239900561.
24. H. Ettoumi, Y. Gao, M. Toumi, and T. Mhiri, Thermal analysis, Raman spectroscopy and complex impedance analysis of Cu2+-doped KDP, *Ionics* **19** (2013) 1067. https://doi.org/10.1007/s11581-013-0926-x.
25. P. Pettersson, and A. Barth, Correlations between the structure and the vibrational spectrum of the phosphate group. Implications for the analysis of an important functional group in phosphoproteins, *RSC Adv.* **10** (2020) 4715. https://doi.org/10.1039/c9ra10366j.
26. E.M. Alkoy, and A. Berksoy-Yavuz, Electrical properties and impedance spectroscopy of pure and copper-oxide-added potassium sodium niobate ceramics, *IEEE Trans. Ultrason. Ferroelectr. Freq. Control.* **59** (2012) 2121. https://doi.org/10.1109/TUFFC.2012.2438.

27. A.K. Dubey, K. Kakimoto, A. Obata, and T. Kasuga, Enhanced polarization of hydroxyapatite using the design concept of functionally graded materials with sodium potassium niobate, *RSC Adv.* **4** (2014) 24601. https://doi.org/10.1039/c4ra02329c.

28. I.M. Hodge, M.D. Ingram, and A.R. West, Impedance and modulus spectroscopy of polycrystalline solid electrolytes, *J. Electroanal. Chem.* **74** (1976) 125. https://doi.org/10.1016/S0022-0728(76)80229-X.

29. B. Singh, S. Kumar, B. Basu, and R. Gupta, Conductivity studies of silver-, potassium-, and magnesium-doped hydroxyapatite, *Int. J. Appl. Ceram. Technol.* **12** (2015) 319. https://doi.org/10.1111/ijac.12167.

30. B. Harihara Venkataraman, and K.B.R. Varma, Frequency-dependent dielectric characteristics of ferroelectric SrBi 2Nb2O9 ceramics, *Solid State Ion.* **167** (2004) 197. https://doi.org/10.1016/j.ssi.2003.12.020.

31. J. P. Gittings, C. R. Bowen, I. G. Turner, F. Baxter, and J. Chaudhuri, Characterisation of ferroelectric-calcium phosphate composites and ceramics, *J. Eur. Ceram. Soc.* **27** (2007) 4187. https://doi.org/10.1016/j.jeurceramsoc.2007.02.120.

32. K. P. Tank, B. V. Jogiya, D. K. Kanchan, and M. J. Joshi, Dielectric properties of pure and strontium doped nano-hydroxyapatite, *Solid State Phenom.* **209** (2014) 151. https://doi.org/10.4028/www.scientific.net/SSP.209.151.

33. P. Lunkenheimer *et al*., Ionic motion in bioactive ceramics investigated by dielectric spectroscopy, *Solid State Ion.* **81** (1995) 129. https://doi.org/10.1016/0167-2738(95)00170-B.

34. C. C. Silva, M. P. F. Graça, M. A. Valente, and A. S. B. Sombra, AC and DC conductivity analysis of hydroxyapatite and titanium calcium phosphate formed by dry ball milling, *J. Non Cryst. Solids.* **352** (2006) 1490. https://doi.org/10.1016/j.jnoncrysol.2006.01.028.

35. G. Garcia-Belmonte, V. Kytin, T. Dittrich, and J. Bisquert, Effect of humidity on the ac conductivity of nanoporous TiO[sub 2], *J. Appl. Phys.* **94** (2003) 5261. https://doi.org/10.1063/1.1610805.

36. A. K. Jonscher, Dielectric relaxation in solids,1st ed.(Chelsea Dielectrics, London, 1983) pp. R57-R70.

37. B. Singh, S. Kumar, B. Basu, and R. Gupta, Enhanced ionic conduction in hydroxyapatites, *Mater. Lett.* **95** (2013) 100. https://doi.org/10.1016/j.matlet.2012.12.074.

38. S. R. Elliott, A theory of a.c. conduction in chalcogenide glasses, *Phil. Mag.* **36** (1977) 1291. https://doi.org/10.1080/14786437708238517.

39. K. K. Bamzai, S. Suri, and V. Singh, Synthesis, characterization, thermal and dielectric properties of pure and cadmium doped calcium hydrogen phosphate, *Mater. Chem. Phys.* **135** (2012) 158. https://doi.org/10.1016/j.matchemphys.2012.04.040.

40. A. K. Jonscher, Dielectric relaxation in solids, *J. Phys. D Appl Phys.* **32** (1999) R57. https://doi.org/10.1088/0022-3727/32/14/201.

41. A. Das and D. Pamu, A comprehensive review on electrical properties of hydroxyapatite based ceramic composites, *Mater. Sci. Eng. C* **101** (2019) 539. https://doi.org/10.1016/j.msec.2019.03.077.

42. F. M. Souza, Electrical Conductivity in the KDP, ADP, and K1-x(NH4)xH2PO4 crystals, *Mat. Res.* **20** (2017) 532. https://doi.org/10.1590/1980-5373-MR-2016-0603.